STTR PHASE I: FINAL TECHNICAL REPORT

ACES Q. C., LC.
CONTRACT NUMBER: FA55005C0094
Topic Number: AF05-T010

Computational Prediction of Kinetic Rate Constants

Rodney J. Bartlett, University of Florida
John Barker, University of Michigan
James M. Ponton, ACES Q.C., LC.
Neil Ostlund, Hypercube, Inc.
Ajith Perera, University of Florida

REPORT DOCUMENTATION PAGE

Form Approved
OMB No. 0704-0188

1. REPORT DATE *(DD-MM-YYYY)*	**2. REPORT TYPE**	**3. DATES COVERED** *(From - To)*
9 June 2006	Phase I Final Summary Report	15 Aug 05 – 14 May 06

4. TITLE AND SUBTITLE
Phase I. Final Technical Report/Final Summary Report.
Computational Prediction of Kinetic Rate Constants

5a. CONTRACT NUMBER
FA9550-05-C-0094

5b. GRANT NUMBER

5c. PROGRAM ELEMENT NUMBER

6. AUTHOR(S)
Bartlett, Rodney J., University of Florida
Barker, John, University of Michigan
Ponton, James M., ACES QC, L.C.
Ostlund, Neil, Hypercube, Inc.
Perera, Ajith, University of Florida

5d. PROJECT NUMBER

5e. TASK NUMBER

5f. WORK UNIT NUMBER

7. PERFORMING ORGANIZATION NAME(S) AND ADDRESS(ES)
ACES QC, L.C.
1421 NW 47th Terrace
Gainesville, FL 32605

8. PERFORMING ORGANIZATION REPORT NUMBER
AFSTTR04

9. SPONSORING / MONITORING AGENCY NAME(S) AND ADDRESS(ES)
AFOSR/NL USAF, AFRL
AF Office of Scientific Research
875 North Randolph St Rm 3112
Arlington, VA 22203

10. SPONSOR/MONITOR'S ACRONYM(S)

11. SPONSOR/MONITOR'S REPORT NUMBER(S)
AFRL-SR-AR-TR-06-0371

12. DISTRIBUTION / AVAILABILITY STATEMENT
Approved for public release; distribution unlimited

13. SUPPLEMENTARY NOTES

14. ABSTRACT
This is the Final Technical Report / Final Phase I Summary Report for the STTR on topic #AF05-T010 entitled "Computational Prediction of Kinetic Rate Constants." In Phase I it has been shown that the combination of electronic structure offered by the ACES program system and the user-friendly interface of HyperChem can be combined together to provide the data required from quantum chemistry to provide thermal rate constants for molecules. The actual rate constant evaluation is accomplished in the new module, ACESRATE, using transition state theory, variational transition state theory, and RRKM. All of these methods were coded into ACESRATE in Phase I. The primary objective of the project was the design and testing of the interface that makes such calculations easy for non-expert users.

15. SUBJECT TERMS
STTR Final Technical Report / Final Phase I Summary Report

16. SECURITY CLASSIFICATION OF:			**17. LIMITATION OF ABSTRACT**	**18. NUMBER OF PAGES**	**19a. NAME OF RESPONSIBLE PERSON**
a. REPORT	**b. ABSTRACT**	**c. THIS PAGE**			Rodney J. Bartlett
U	U	U	U	28	**19b. TELEPHONE NUMBER** *(include area code)* 352-392-6974

Standard Form 298 (Rev. 8-98)
Prescribed by ANSI Std. Z39.18

1 Project Objectives

In the words of the RFP, the project objective was to "develop seamless, easy to use, efficient code to calculate electronic wave functions and potential energy surfaces of molecules and predict kinetic rate constants for reactions *a priori*."

This was to be accomplished by:

- Building upon the widely used, user-friendly program HyperChem
- Tying it to the very high-level quantum chemical program ACES
- Investigating the feasibility of providing tools for the facile application of high-powered quantum mechanical methods to rate constant determination by non-expert users
- Assessing accuracy and limitations of the existing theory and identifying improvements to be added in Phase II.

2 Work Performed

- Implemented transition state theory (TST) and variational transition state theory (VTST) into the ACESRATE program to enable electronic structure results made with any of the extensive capabilities of the ACES program system to be seamlessly connected to provide thermal rate constants for gas phase reactions.
- Provided interfaces between ACES, ACESRATE, and HyperChem to enable all to be executed from one point of control, the user-friendly HyperChem program with its GUI, and to visualize results of the calculations with HyperChem.
- Implemented RRKM for unimolecular rate constants to complement TST and VTST for rate constant determination.
- Put all the above into a user-friendly form to initiate a new software product that will be marketed as a part of the HyperChem and ACES program systems.

3 Results Obtained

In Phase I reactions such as $\tau OH+CH_4$, $H+CH_4$, $\tau Cl + CH_4$, and others were studied using MP2 electronic structure results for energy surfaces and associated parameters. We also used empirically corrected (SAC) MP2 to assess the differences. Results for many such reactions have been done in prior reports, and two are shown below. For $\tau OH+CH_4$ note the importance of the hindered rotor correction and the tunneling correction (the SCT result is from

Truhlar, but will be added to ACESRATE in Phase II). Compare that to τCl + CH_4. Among other observations, ACES and ACESRATE reproduced the identical results from the POLYRATE package, attesting to the veracity of our VTST and MP2 (SAC) results.

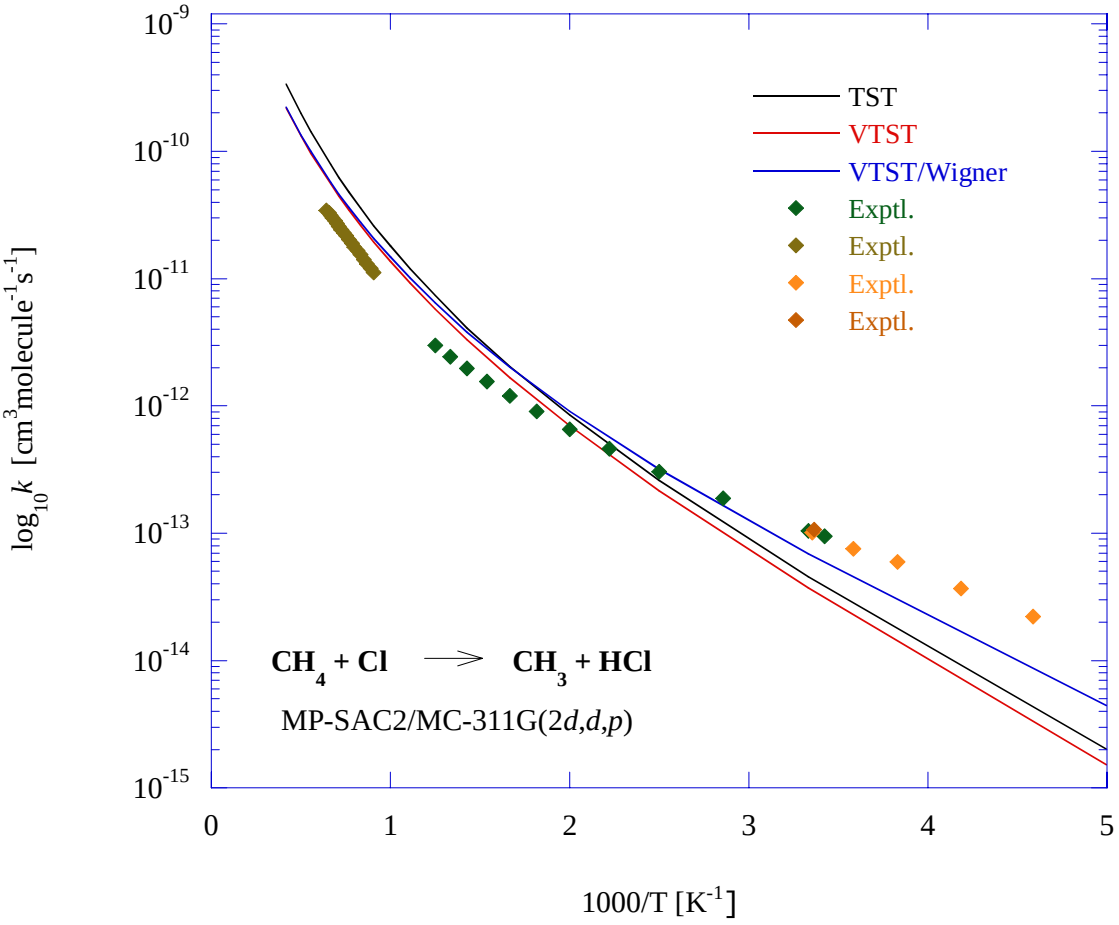

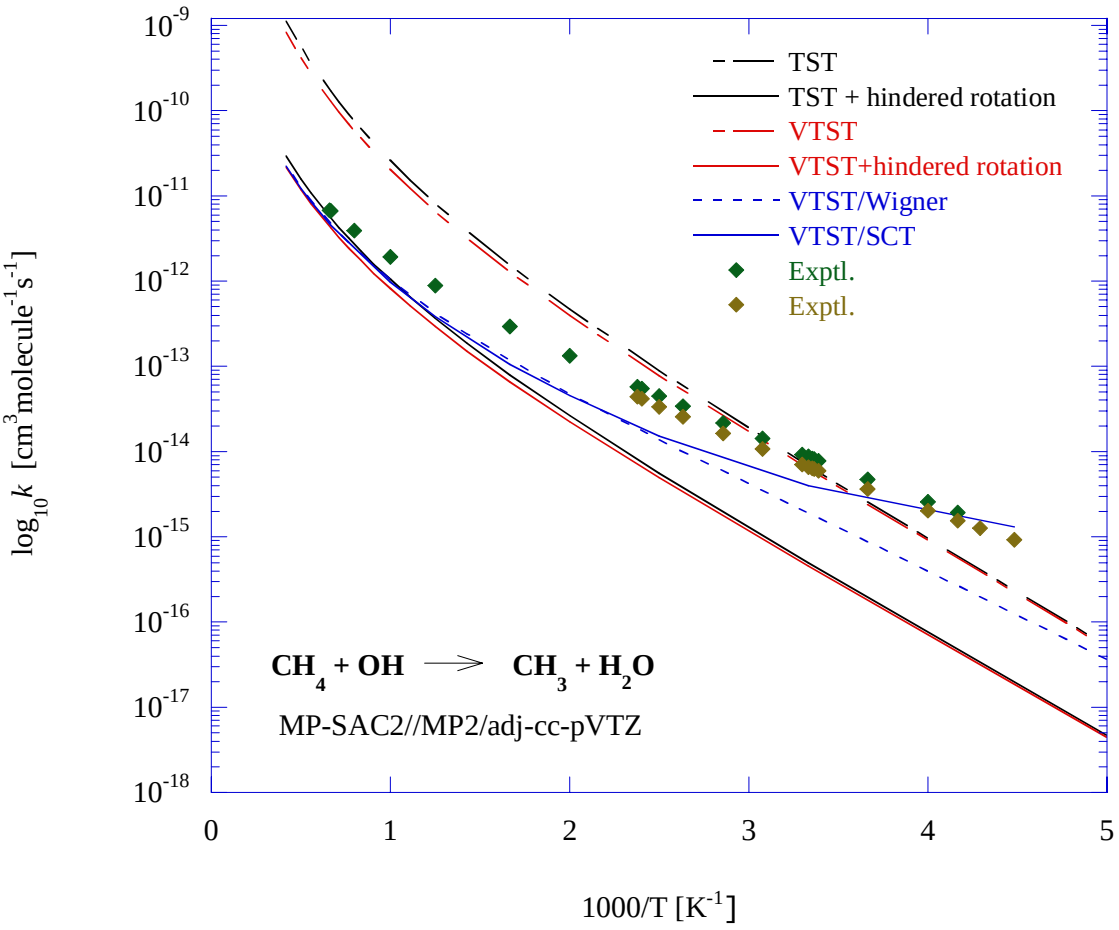

4 Problem Description (A real world example.)

Since international treaties have mandated destruction of existing chemical warfare (CW) agents, and incineration is an attractive means of accomplishing their destruction, the thermal decomposition mechanisms of CW agents, precursors and their simulants must be known to assure that the thermal destruction is effective and safe (C&E News 84(16) 27 April 17, 2006). The extreme toxicity of these CW agents makes it challenging to carry out conventional experiments, and a complimentary approach is to evaluate the mechanisms, rate constants and other critical data (for example, the structures of intermediates) using theoretical chemistry.

As a proof of principle of the phase-I developments toward the avowed AFOSR goal of computng *a priori* rate constants, and to allow evaluation of the methodology and software, we have applied electronic structure and reaction kinetics calculations to triethyl phosphate (TEP, CAS # 78-40-0) and methylphosphonic difluoride (DF, CAS # 676-99-3), at the suggestion of Bryan

Shiloff, (**Air Force Nuclear Weapons and Counterproliferation Agency Advanced Technology Division, AFNWCA/ATDA, Kirtland AFB NM**). The structures of DF and TEP are shown below.

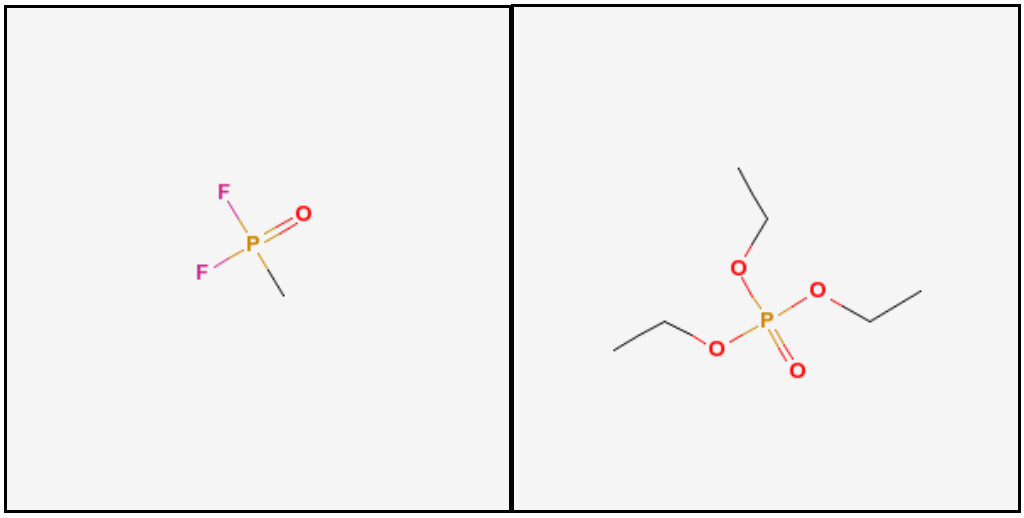

DF TEP

In addition to setting the phase-I benchmarks, the results of the electronic structure and reaction kinetics analysis for this 'real-world' example will be compared to the previously predicted or experimentally determined values in order to validate the calculations and to identify weak elements that require attention in Phase II. Based on the results of the initial study of DF and TEP, additional test cases can be identified and applied for further evaluation of methods and software. After the validation is complete, the applications could be extended to other chemical warfare related compounds where predictive modeling would be crucial in determining the neutralization conditions for chemical agents.

5 Phase-I Calculations

In this report, we focus on the primary stage of the decomposition of TEP and DF. An important element of our approach is that we intend to seamlessly enable virtually all applicable levels of electronic structure and reaction-path kinetics to be applied to a chosen system. Furthermore, we expect that that the results will be obtained in an interactive mode using a low-level of theory which will then become the starting point for the next level, that might require execution in the background using much faster resources, but from one point of control, until we

obtain an expected accuracy defined by ‘calibrations’ of that level of theory for many applications.

In the example of TEP, we apply a relatively high level theoretical treatment to the crucial steps, while limiting the secondary stages to a lower level theoretical survey for the structures to map out most of the mechanism. The latter will be revised at a later stage. Nonetheless, the comparative energetics of the secondary stages are computed at high levels of coupled-cluster theory to obtain accurate thermodynamic data.

Our calculations are in agreement with the generally accepted primary stages of decomposition of the two species:

I) Triethyl Phosphate:

$$(C_2H_5O)_3PO \rightarrow PO(OH)(C_2H_5O)2 + C_2H_4 \quad (1)$$

$$(C_2H_5O)_2PO(OH) \rightarrow C_2H_4 + (C_2H_5O)PO(OH)_2 \quad (2)$$

$$(C_2H_5O)PO(OH)_2 \rightarrow C_2H_4 + PO(OH)_3 \quad (3)$$

$$(C_2H_5O)PO(OH)_2 \rightarrow H2O + (C_2H_5O)P(O)_2 \quad (3')$$

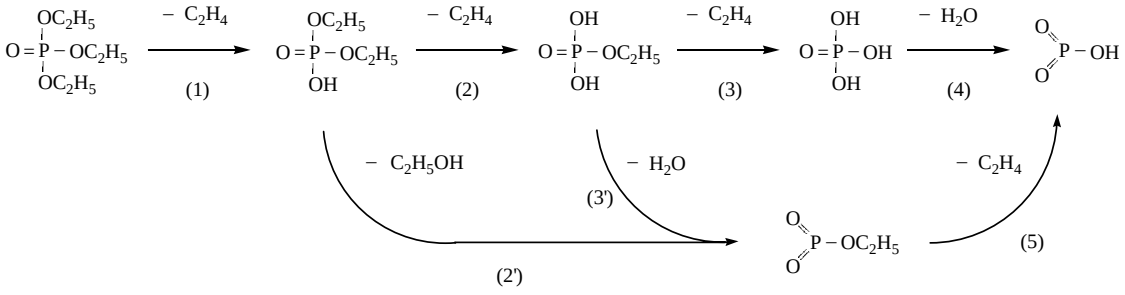

I’) A model compound $(C_2H_5O)PO(F)_2$:

$$(C_2H_5O)PO(F)_2 \rightarrow C_2H_4 + PO(OH)F_2 \quad (1')$$

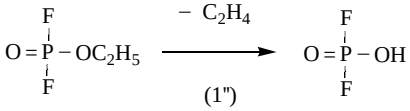

II) Methylphosphonic Difluoride:

$$CH_3P(O)F_2 \rightarrow \cdot CH_3 + \cdot P(O)F_2$$

Specifically, the structures of the reactants, transition state and products of reaction (1) were obtained using density functional theory (B3LYP) and they are being used as a starting point for a more accurate coupled cluster (CC) treatment, which will be done later. However, the energetics of the TEP decomposition intermediates (see Scheme I) are evaluated at CCSD(T) using the structures optimized using DFT methods. In the case of DF, the structures and energetics reported here are all obtained at CCSD(T) level.

We were able to obtain a PM3 semi empirical TS from HyperChem, but despite that starting guess, found it much harder to locate the corresponding DFT results. To demonstrate the difficulty in finding a saddle point on the multi-dimensional surface as complicated as TEP, we report the steps required to locate the DFT-B3LYP TS.

Transition state searches, via optimization to a first-order saddle point using eigenvector following, using DFT; proved quite troublesome even with using analytical second derivatives. For example, straight forward calculations for the TEP transition state leading to ethylene elimination provides three imaginary frequencies all within approximately 10 cm^{-1} of each other and thus not clearly providing a mode which corresponds to a reaction coordinate. We also experienced difficulties in the water elimination from an intermediate created during the decomposition of TEP due to methyl rotations. Due to these difficulties we adopted the following strategy to assist in the transition state search.

Starting with a simplified model of TEP in which two of the ethoxy groups are replaced by fluorine atoms, $F_2POOCH_2CH_3$, we optimized the geometry starting from a semi-empirical theory guess. For this model compound we were then able to do a straight-forward transition state search which was successful, as shown in A of the figure. The next step was to replace one of the fluorine atoms by a hydroxyl group and optimize the positions of the atoms in the hydroxyl group while keeping the other atoms fixed. Then a transition state search is performed in which all atom positions are allowed to vary leading to B in the figure. This procedure of constrained minimization followed by unconstrained transition state optimization is carried out as we build to TEP, next by replacing the hydroxyl by an ethoxy. This series of steps is carried out for the other fluorine and are shown in parts C, D, and E of the figure. As a final result, part E, we fine one of the many transition states of TEP. All structures shown are for transition states determined using DFT//B3LYP//6-31G*.

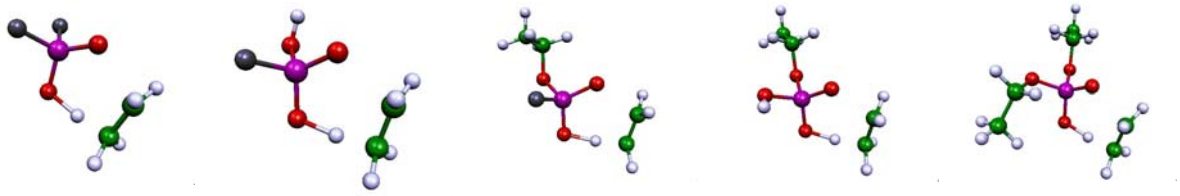

A B C D E

These data are used for chemical kinetics analysis such as transition state theory and RRKM methods, to generate Arrhenius plots, and to extract the activation energies and pre-exponential factors.

6 Results

Table 1 shows the rate constant of the primary decomposition path of TEP over a range of temperatures computed using RRMK and TST methods using the electronic structure data computed at the PM3 and DFT level of theory. The corresponding Arrhenius plots are shown in Figures 1 and 2; Figure 1 spans the full temperature range and the other spans a shorter temperature change that is typical of experimental conditions in order to amplify the features in the region of experimental interest. Both the RRKM and TST results were obtained using codes developed during Phase I of this project. Both use well-established theory and have been tested for accuracy. The TST calculations are based on the usual ratios of partition functions, while the RRKM code takes the usual approach of calculating the microcanonical rate constants (k(E)) from sums and densities of states (exact counts with a 10 cm^{-1} energy grain) and then averaging over the thermal energy distribution to obtain k_∞ (the high pressure limit) [W. Forst, Unimolecular Reactions. A Concise Introduction. (Cambridge University Press, Cambridge, 2003)]. The pressure dependent rate constants (Figures 2, 5, 6, 8, and 11) are based on the RRKM integral and strong collision approximation (unit collision efficiency), since no energy transfer information is available for these species.

Table 1: TST and RRKM rate constants (in s^{-1}) for TEP decomposition reaction process (1).

T (K)	PM3		DFT		Experiment		
	k_{TST}	k_{RRKM}	k_{TST}	k_{RRKM}	Glaude[a]	Tsang[b]	Zeger[c]
100	4.643e-93	4.681e-93	5.747e-80	5.716e-80	2.79e-86	1.24e-85	2.57e-90
200	2.291e-40	2.300e-40	2.898e-34	2.891e-34	8.84e-37	1.11e-36	1.60e-38
300	9.278e-23	9.303e-23	5.210e-19	5.201e-19	2.80e-20	2.31e-20	2.95e-21
400	6.536e-14	6.549e-14	2.390e-11	2.387e-11	4.98e-12	3.33e-12	1.27e-12
500	1.427e-08	1.429e-08	1.007e-06	1.006e-06	4.44e-07	2.62e-07	1.91e-07
600	5.404e-05	5.412e-05	1.277e-03	1.276e-03	8.85e-04	4.81e-04	5.43e-04
700	1.997e-02	1.999e-02	2.171e-01	2.169e-01	2.01e-01	1.03e-01	1.59e-01
800	1.711e+00	1.713e+00	1.045e+01	1.045e+01	1.18e+01	5.77e+00	1.13e+01
900	5.515e+01	5.520e+01	2.163e+02	2.162e+02	2.80e+02	1.32e+02	3.09e+02
1000	8.941e+02	8.949e+02	2.470e+03	2.469e+03	3.52e+03	1.62e+03	4.37e+03
1100	8.780e+03	8.787e+03	1.827e+04	1.826e+04	2.80e+04	1.26e+04	3.83e+04
1200	5.913e+04	5.918e+04	9.745e+04	9.741e+04	1.57e+05	6.93e+04	2.33e+05
1300	2.978e+05	2.980e+05	4.037e+05	4.035e+05	6.79e+05	2.94e+05	1.08e+06
1400	1.193e+06	1.193e+06	1.370e+06	1.370e+06	2.37e+06	1.02e+06	3.99e+06
1500	3.976e+06	3.979e+06	3.962e+06	3.961e+06	7.03e+06	2.97e+06	1.24e+07

[a] Calculated from Arrhenius expression obtained for temperature range 700-900K and specifically for the reaction process (1); Proceedings of the Combustion Institute, Volume 28, 2000, 1749-1756.

[b]Calculated from Arrhenius expression obtained for temperature range 840-940K; See *Combust. Sci. and Tech.*, 1998, Vol. 138, 85-103..

[c]Calculated from Arrhenius expression obtained for temperature range 706-854K; *Combust. Sci. and Tech.*, 1998, Vol. 138, 85-103.

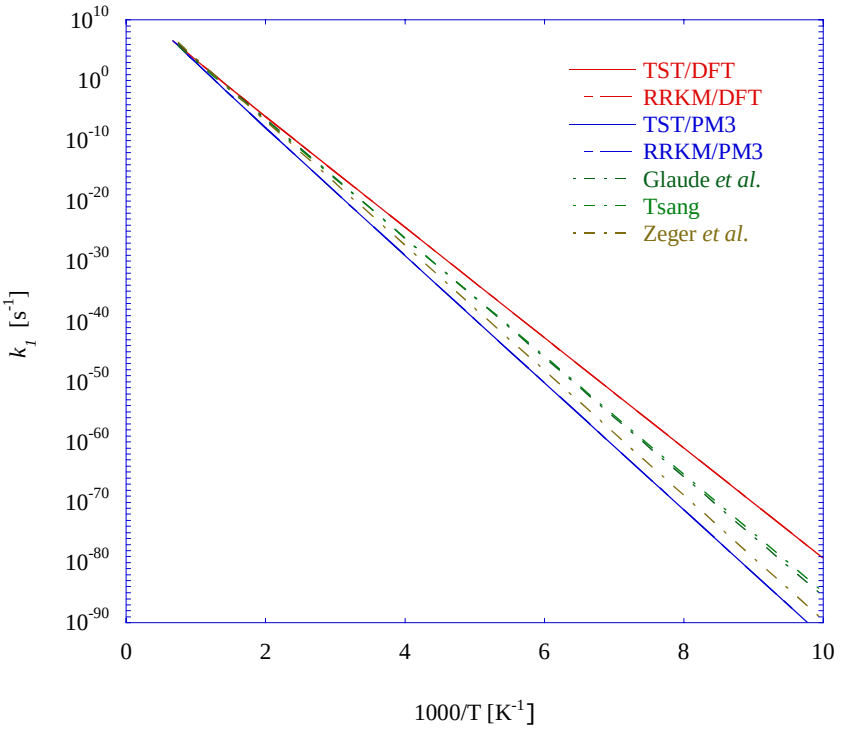

(a)

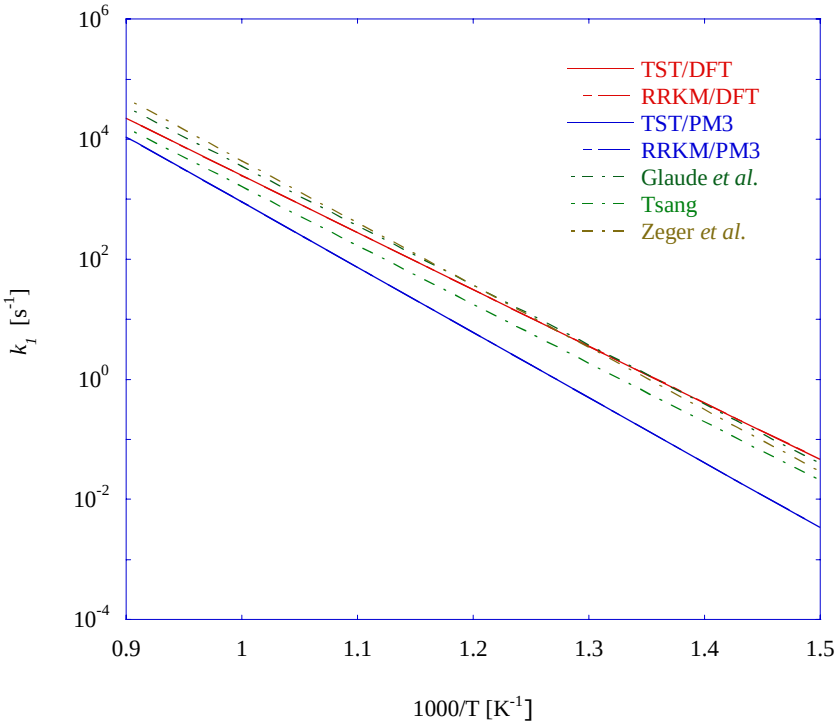

(b)

Figure 1: Plots of rate constant vs 1000/T for TEP decomposition process (1). The plot (a) corresponds to a temperature range from 100K to 1000K or higher while the plot (b) correspond to the temperature range of the experiment ~700K to 900K.

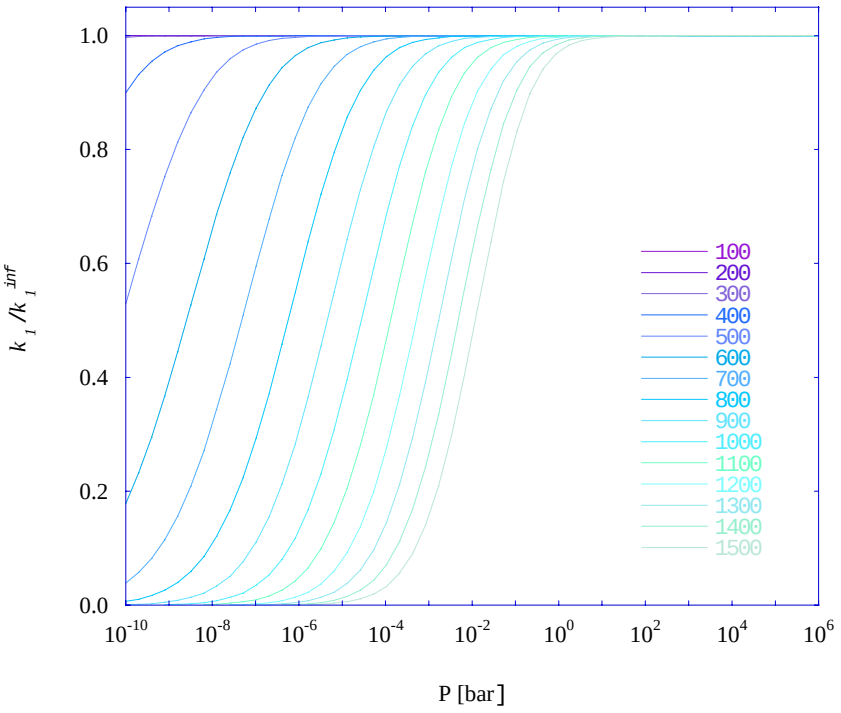

(a)

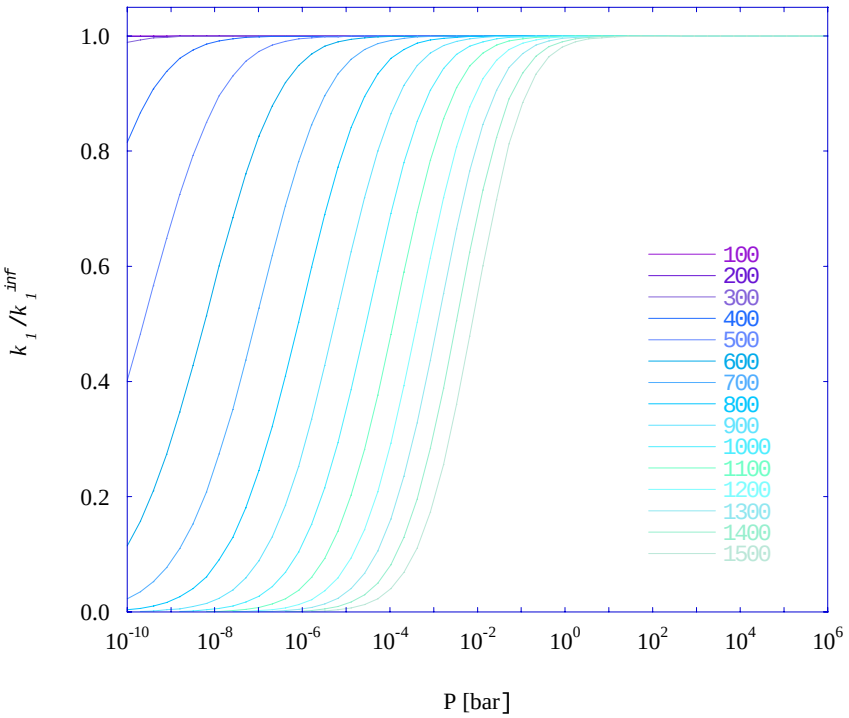

(b)

Figure 2: Plots of rate constant ratio with respect to infinite pressure limit (k/k^{inf}) vs Pressure (P) for TEP decomposition process (1): (a) PM3 calculation. (b) DFT calculation.

In theory, the high pressure limiting RRKM rate constant (k_∞) should be equal to the canonical TST rate constant. In practice, two entirely different numerical approaches are taken, each with its own set of approximations and imperfections. Thus the level of agreement between the two approaches provides a test of both. The excellent agreement between the RRKM and TST rate constants in the tables gives us confidence that both numerical calculations are performing exceptionally well for this system, which has an intrinsic energy barrier.

The primary decomposition path of TEP (1) has been widely studied and three different experimental rate constants are available. The computed rate constant at 500K computed with both PM3 and DFT is in agreement with all three experimental values, although the A-factors and activation energies obtained from the two levels of electronic structure theory are significantly different. This is not surprising, because the PM3 method is well known to be of only qualitative usefulness, although it is very computationally efficient. Energies calculated using DFT are more accurate, but may still be in error by a few (2-3 kcal/mol?). Because of the different activation energies, agreement between theory and experiment (and also among the three experiments) deteriorates because of the different Arrhenius parameters. As the temperature increases the variations among the 3 experimental values, and their deviation from the computed values are moderate compared to the behavior observed for the lower temperatures. As shown in Table 5, the computed activation energy (using the Arrhenius plot) and the Arrhenius A-factor for the primary decomposition using DFT/TST (or RRKM) is 42.080 Kcal/mol and 3.550×10^{12} s^{-1} respectively. The corresponding PM3/TST values are 48.514 Kcal/mol and 3.214×10^{12} s-1.

The DFT results are greatly preferred over the PM3 results. Calculated A-factors depend on vibrational frequencies and molecular structures, which are calculated relatively accurately using DFT. The calculated A-factors are one to two orders of magnitude larger than the experimental values and they are quite consistent with the expected tight transition state [S. W. Benson, Thermochemical Kinetics, 2nd ed. (Wiley, New York, 1976)]. The computed activation energy is about 3, 2 and 5 Kcal/mol lower than three experimental values 45.3, 44.8 and 47.4 Kcal/mol, which differ by almost 3 kcal mol^{-1}. Considering the limited experimental temperature ranges and the fact that the A-factor and associated activation energy are usually statistically correlated in a least-squares analysis, such discrepancies are not unusual.

In Table 2, we report the computed rate constants with both TST and RRKM over a range of temperatures. The corresponding Arrhenius plots are shown in Figures 3 and 4 for secondary decomposition reactions of TEP (2) and (3), respectively. The computed activation energies and the Arrhenius A-factors are shown. There are no experimental results available for these secondary decomposition reactions. On the basis of the agreement shown for the primary decomposition, one might argue that DFT/TST results must be accurate, but it

should be recognized that the activation energies may be in error by 2-3 kcal mol^{-1}. Computed A-factors are usually much more reliable than activation energies. Furthermore, the exponential dependence of thermal rate constants on the activation energy amplifies the errors. Table 3 shows the same kinetic data for the model compounds that are used in the early stages of the study. There is no experimental rate data available for the model system in order to make any assessments of the accuracy of the computed results.

Table 2: TST and RRKM rate constants (in s^{-1}) for TEP decomposition reaction (2) and (3').

T (K)	Reaction (2)		Reaction (3')	
	k_{TST}	k_{RRKM}	k_{TST}	k_{RRKM}
100	1.140e-79	1.123e-79	1.831e-74	1.838e-74
200	4.205e-34	4.175e-34	1.448e-31	1.450e-31
300	7.047e-19	7.012e-19	2.790e-17	2.793e-17
400	3.145e-11	3.134e-11	3.829e-10	3.832e-10
500	1.307e-06	1.303e-06	7.312e-06	7.317e-06
600	1.643e-03	1.639e-03	5.225e-03	5.228e-03
700	2.778e-01	2.772e-01	5.723e-01	5.727e-01
800	1.333e+01	1.330e+01	1.944e+01	1.945e+01
900	2.749e+02	2.745e+02	3.029e+02	3.030e+02
1000	3.132e+03	3.128e+03	2.734e+03	2.735e+03
1100	2.313e+04	2.310e+04	1.659e+04	1.660e+04
1200	1.232e+05	1.231e+05	7.477e+04	7.480e+04
1300	5.098e+05	5.092e+05	2.679e+05	2.680e+05
1400	1.728e+06	1.727e+06	8.018e+05	8.021e+05
1500	4.995e+06	4.990e+06	2.077e+06	2.077e+06

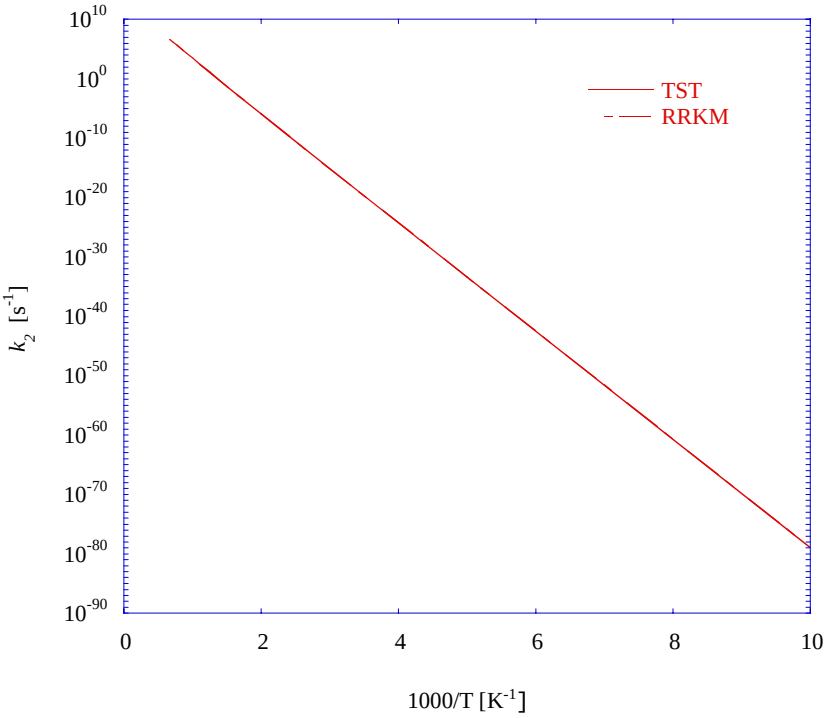

Figure 3: Plot of rate constant vs 1000/T for TEP decomposition, reactions (2)

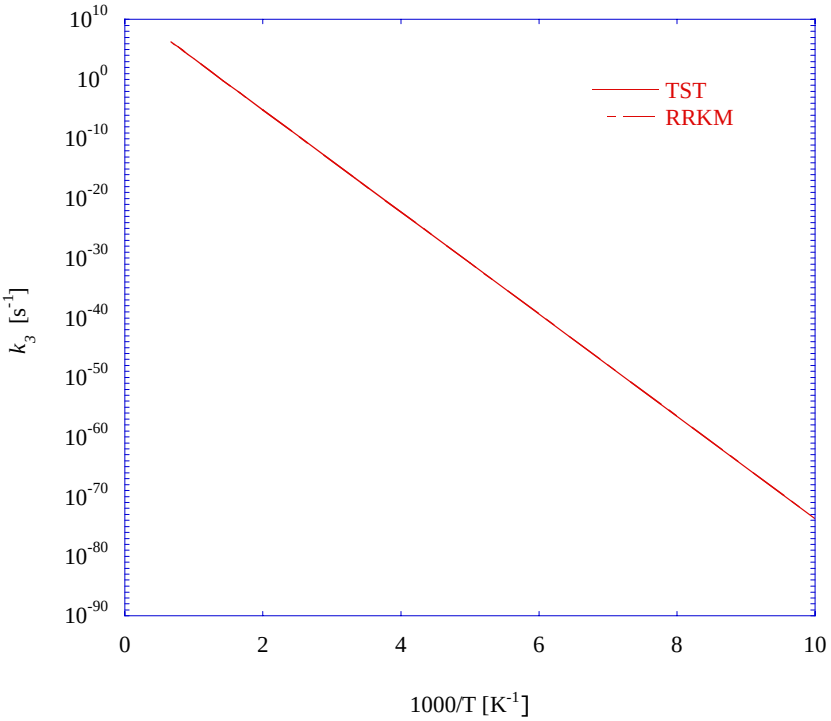

Figure 4: Plot of rate constant vs 1000/T for TEP decomposition, reactions (3')

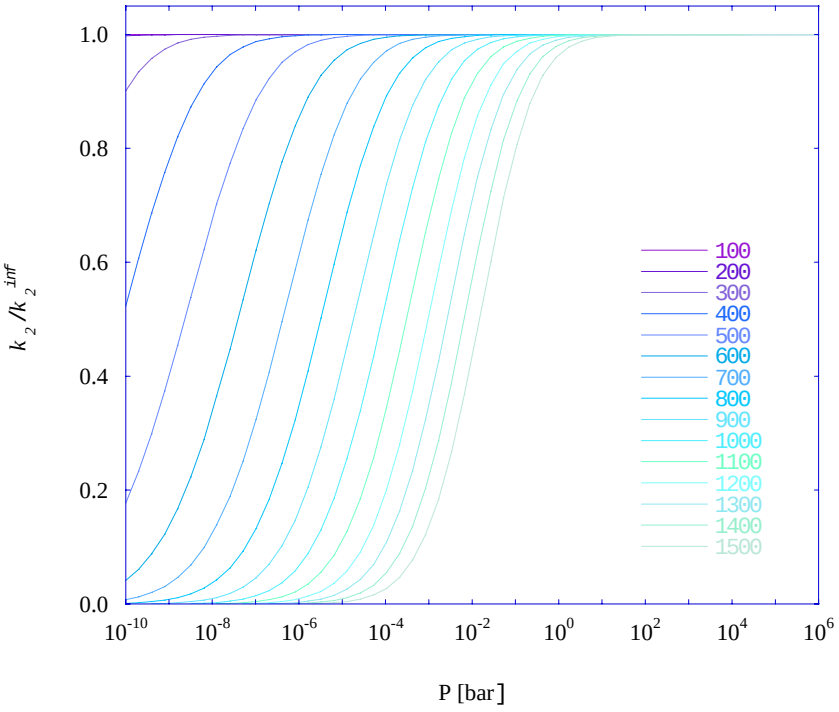

Figure 5: Plots of rate constant ratio with respect to infinit pressure limit (k/k^{inf}) vs Pressure (P) for TEP decomposition process (2).

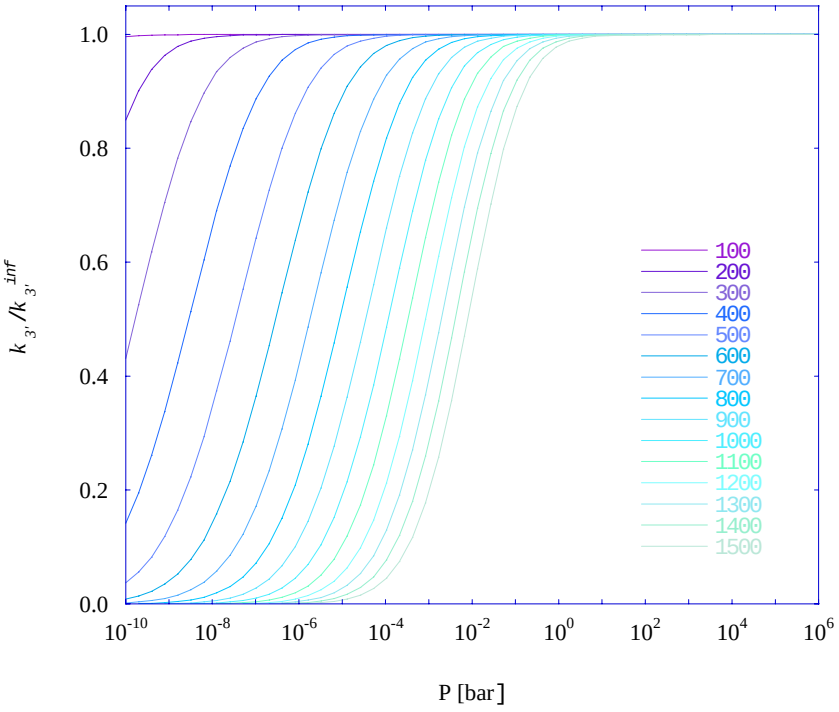

Figure 6: Plots of rate constant ratio with respect to infinite pressure limit (k/k^{inf}) vs Pressure (P) for TEP decomposition process (3').

Table 3: TST and RRKM rate constants (in s^{-1}) for model TEP decomposition reaction (1").

T (K)	Reaction (1")	
	k_{TST}	k_{RRKM}
100	4.778e-71	4.834e-71
200	7.679e-30	7.726e-30
300	4.603e-16	4.622e-16
400	3.897e-09	3.910e-09
500	5.974e-05	5.990e-05
600	3.862e-02	3.870e-02
700	4.058e+00	4.066e+00
800	1.363e+02	1.365e+02
900	2.130e+03	2.133e+03
1000	1.943e+04	1.946e+04
1100	1.197e+05	1.199e+05
1200	5.479e+05	5.487e+05
1300	1.995e+06	1.997e+06
1400	6.061e+06	6.069e+06
1500	1.593e+07	1.595e+07

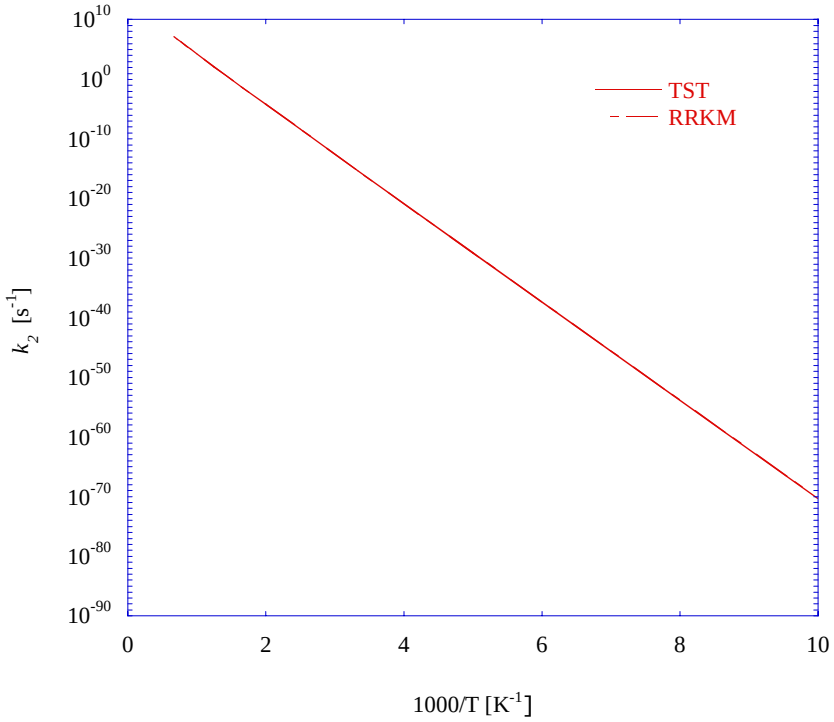

Figure 7: Plot of rate constant vs 1000/T for TEP decomposition, reactions (1")

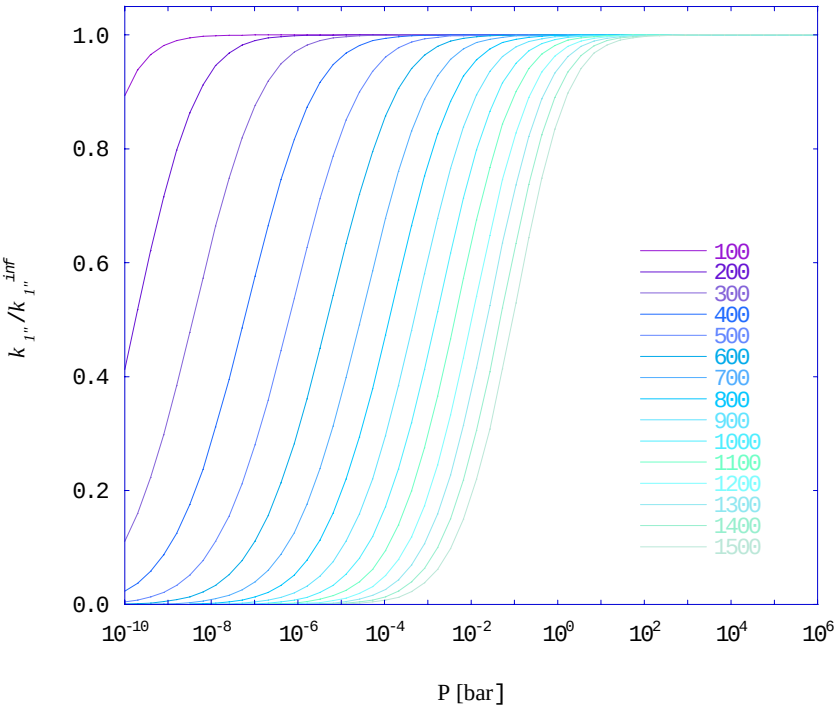

Figure 8: Plots of rate constant ratio with respect to infinite pressure limit (k/k^{inf}) vs Pressure (P) for TEP decomposition process (1").

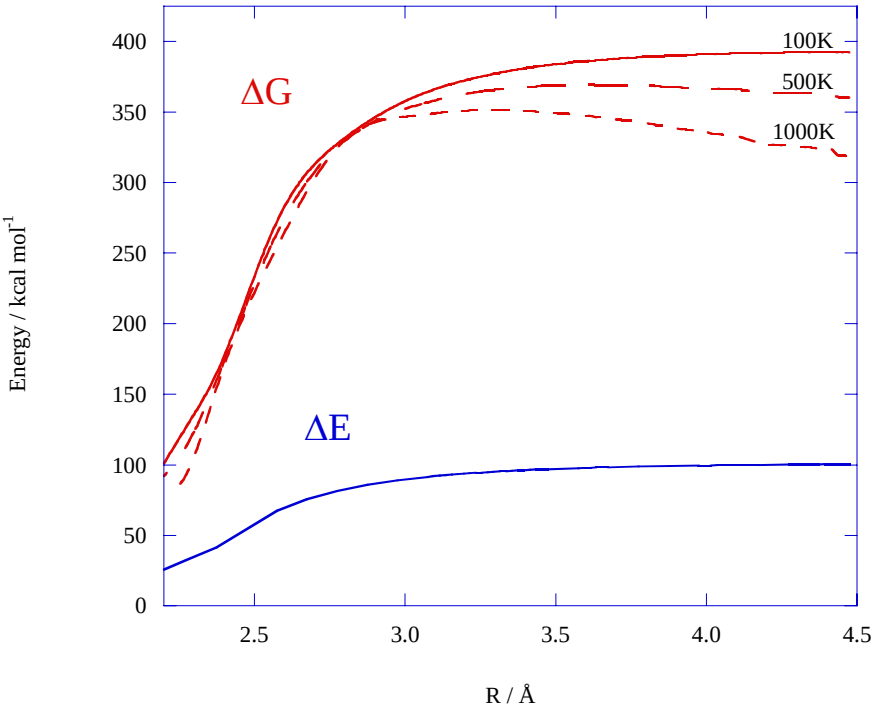

Figure 9: Born-Oppenheimer potential (ΔE) and Gibbs free energy (ΔG) variation for temperature 100K, 500K and 1000K, respectively, with respect to P–C bond length for the dissociation process of DF.

In Table 4, the same set of data as for the reactions (1), (2) and (3) is shown for the primary decomposition of DF as proposed by photo dissociation studies. This system differs from TEP, since the DF reaction is a bond fission, which is expected to have a loose transition state. The rate constants were calculated using variational TST, according to which the transition state is located at the point of maximum free energy difference (ΔG) as the bond is extended. Because the variational feature is not yet fully implemented in the RRKM code module, we calculated RRKM rate constants at the geometries optimized by the VTST model. Both VTST and RRKM results show very good agreement with each other as shown in Table 4 and Figure 10. Since the photodissociation only involves a bond fission, and for most bond fission reactions there is no “intrinsic energy barrier” (no local minimum in the potential energy path), but it is still necessary to supply energy to overcome the thermodynamic energy difference (bond dissociation energy) between the stable reactants and the separated fragments. Because of that, the rate constant for “barrier-less” reaction increase with the temperature. The transition state is in general defined as the position where the free energy of the activation is a maximum. For reactions with intrinsic energy barrier, the maximum free energy and TS is found at (or very near) the top of the intrinsic energy barrier. For barrier-less reactions, the maximum free energy occurs at a distance that depends on the temperature. For barrier less reactions, the Arrhenius plot is usually curved and the activation energy is defined as the local slope on the plot and it is temperature dependent. The activation energy

computed for DF (Table 5) using the Arrhenius plot is 94.954 Kcal/mol and the A factor is 8.168 x10^{15} s^{-1}.

For this reaction, the calculated A-factor is in the range expected for a loose transition state [S. W. Benson, Thermochemical Kinetics, 2nd ed. (Wiley, New York, 1976)]. The large calculated activation energy is generally consistent with the bond dissociation energy, as expected, but it must be remembered that the calculated energies may be in error by ~ 2-3 kcal mol^{-1}.

Table 4: TST and RRKM rate constants (in s^{-1}) for $CH_3P(O)F_2$ → $\cdot CH_3$ + $\cdot P(O)F_2$ (DF) decomposition reaction.

T (K)	k_{TST}	k_{RRKM}
100	1.125e-192	1.137e-192
200	9.449e-88	9.505e-88
300	4.517e-54	4.508e-54
400	1.097e-36	1.099e-36
500	2.704e-26	2.715e-26
600	2.186e-19	2.186e-19
700	1.759e-14	1.761e-14
800	7.753e-11	7.747e-11
900	5.218e-08	5.226e-08
1000	9.177e-06	9.194e-06

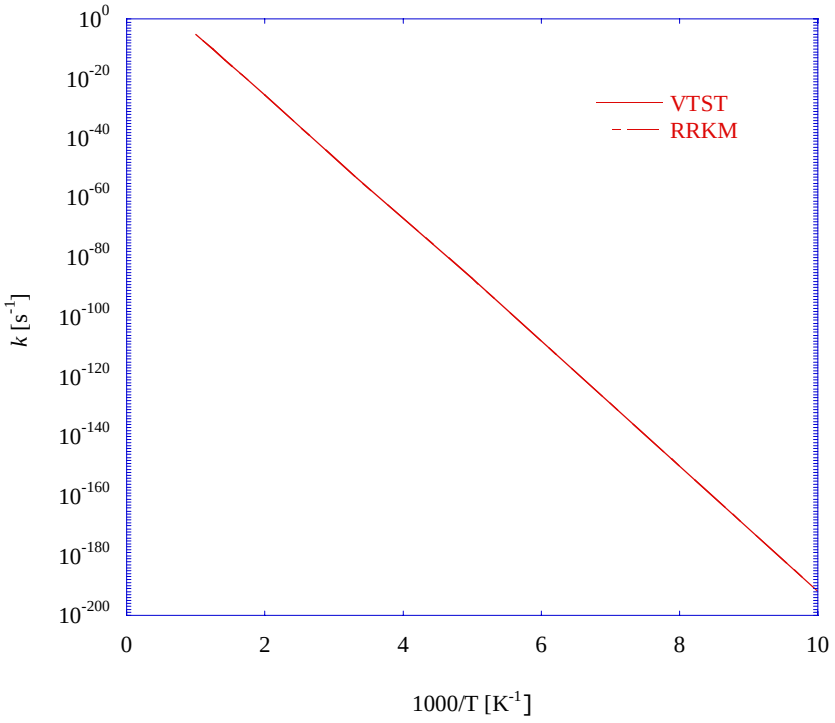

Figure 10: Plot of rate constant vs 1000/T decomposition of DF.

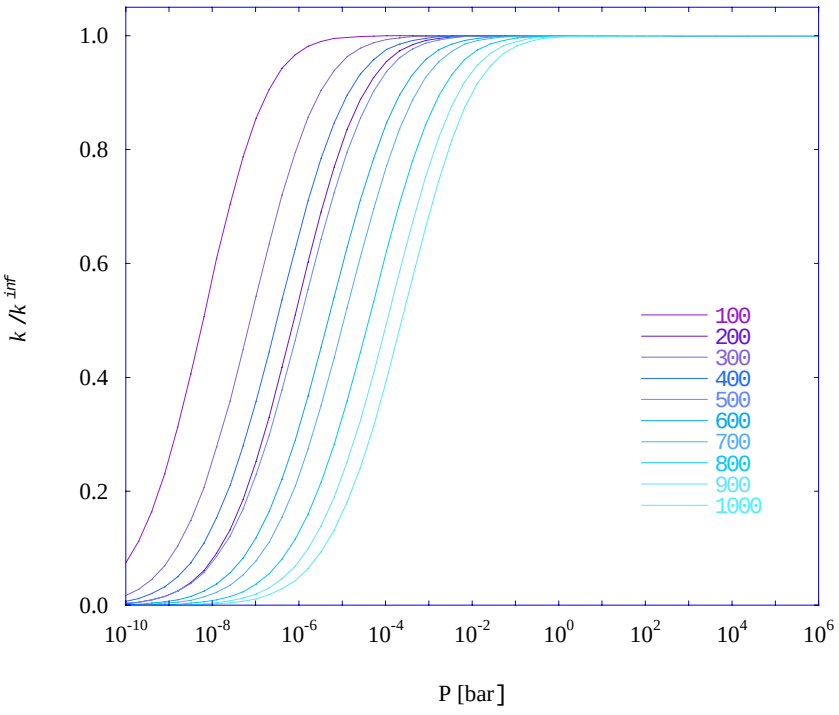

Figure 11: Plots of rate constant ratio with respect to infinite pressure limit (k/k^{inf}) vs Pressure (P) for decomposition of DF.

Table 5. Pre-exponential factor (A in s^{-1}) and activation energy (E_a in kcal mol^{-1}) of Arrhenius expression of rate constants [k=Aexp(–E_a/RT)] for TEP decomposition reaction process (1), (2), (3') and (1") and DF decomposition reaction. DFT (in parenthesis PM3) values for TEP decomposition reaction and MP2 values for DF decomposition.

Reaction	TST		RRKM		Experiment	
	A	E_a	A	E_a	A	E_a
TEP						
(1)	3.550×10^{12} (3.214×10^{15})	42.080 (48.514)	3.550×10^{12} (3.214×10^{13})	42.081 (48.513)		
Glaude *et al.*					2.8×10^{13}	45.3
Tsang					1×10^{13}	44.8
Zeger *et al.*					1×10^{14}	47.4
(2)	4.259×10^{12}	41.987	4.263×10^{12}	41.990		
(3')	1.043×10^{12}	39.236	1.043×10^{12}	39.235		
(1")	3.040×10^{12}	37.545	3.564×10^{12}	38.006		
DF						
	8.168×10^{15}	94.954	8.160×10^{15}	94.952		

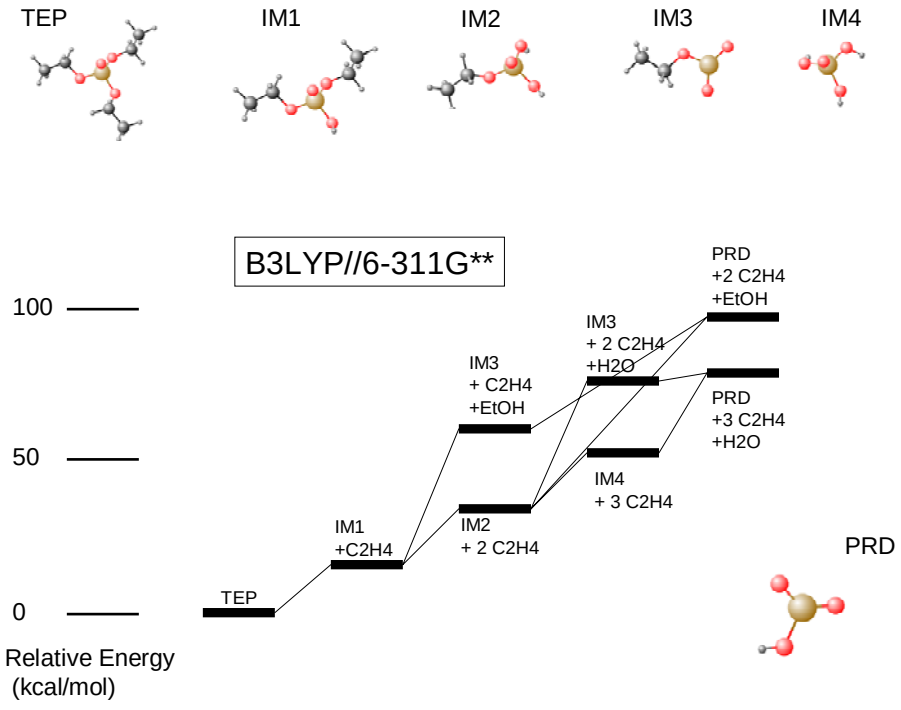

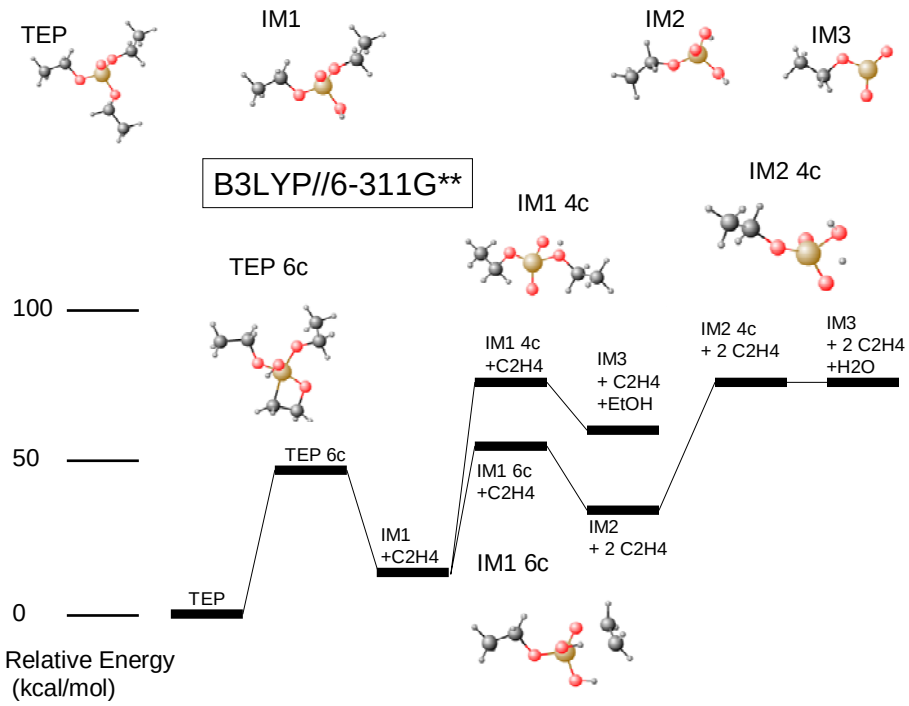
TEP
IM1
IM2
IM3
B3LYP//6-311G**
IM2 4c
IM1 4c
TEP 6c
100
50
0
IM1 4c
+C2H4
IM3
+ C2H4
+EtOH
IM2 4c
+ 2 C2H4
IM3
+ 2 C2H4
+H2O
TEP 6c
IM1 6c
+C2H4
IM1
+C2H4
IM2
+ 2 C2H4
IM1 6c
TEP
Relative Energy
(kcal/mol)

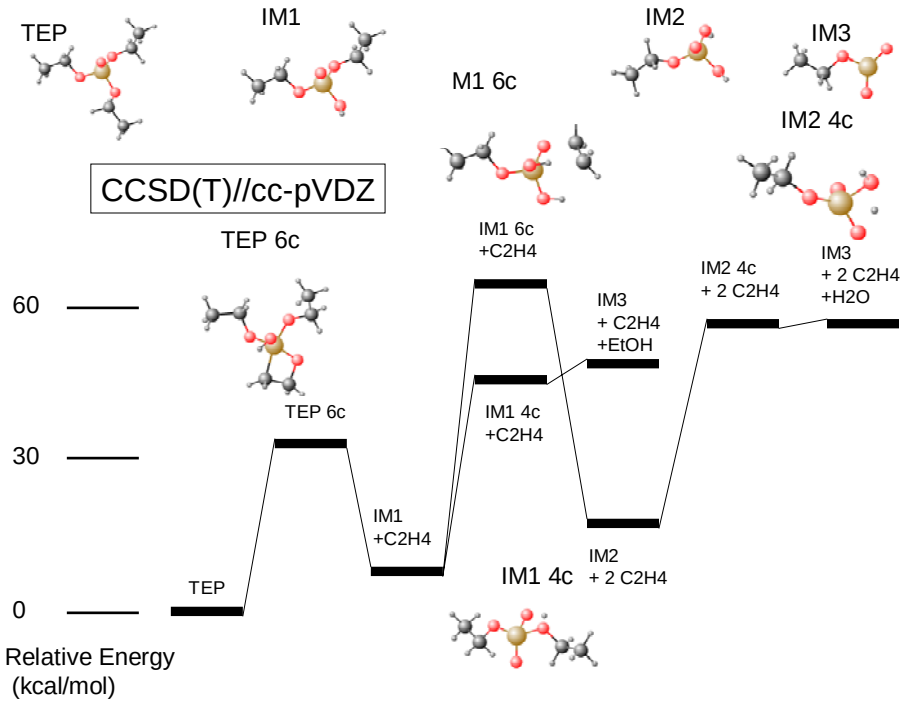
TEP
IM1
IM2
IM3
M1 6c
IM2 4c
CCSD(T)//cc-pVDZ
IM1 6c
+C2H4
TEP 6c
IM2 4c
+ 2 C2H4
IM3
+ 2 C2H4
+H2O
60
30
0
IM3
+ C2H4
+EtOH
IM1 4c
+C2H4
TEP 6c
IM1
+C2H4
IM2
+ 2 C2H4
IM1 4c
TEP
Relative Energy
(kcal/mol)

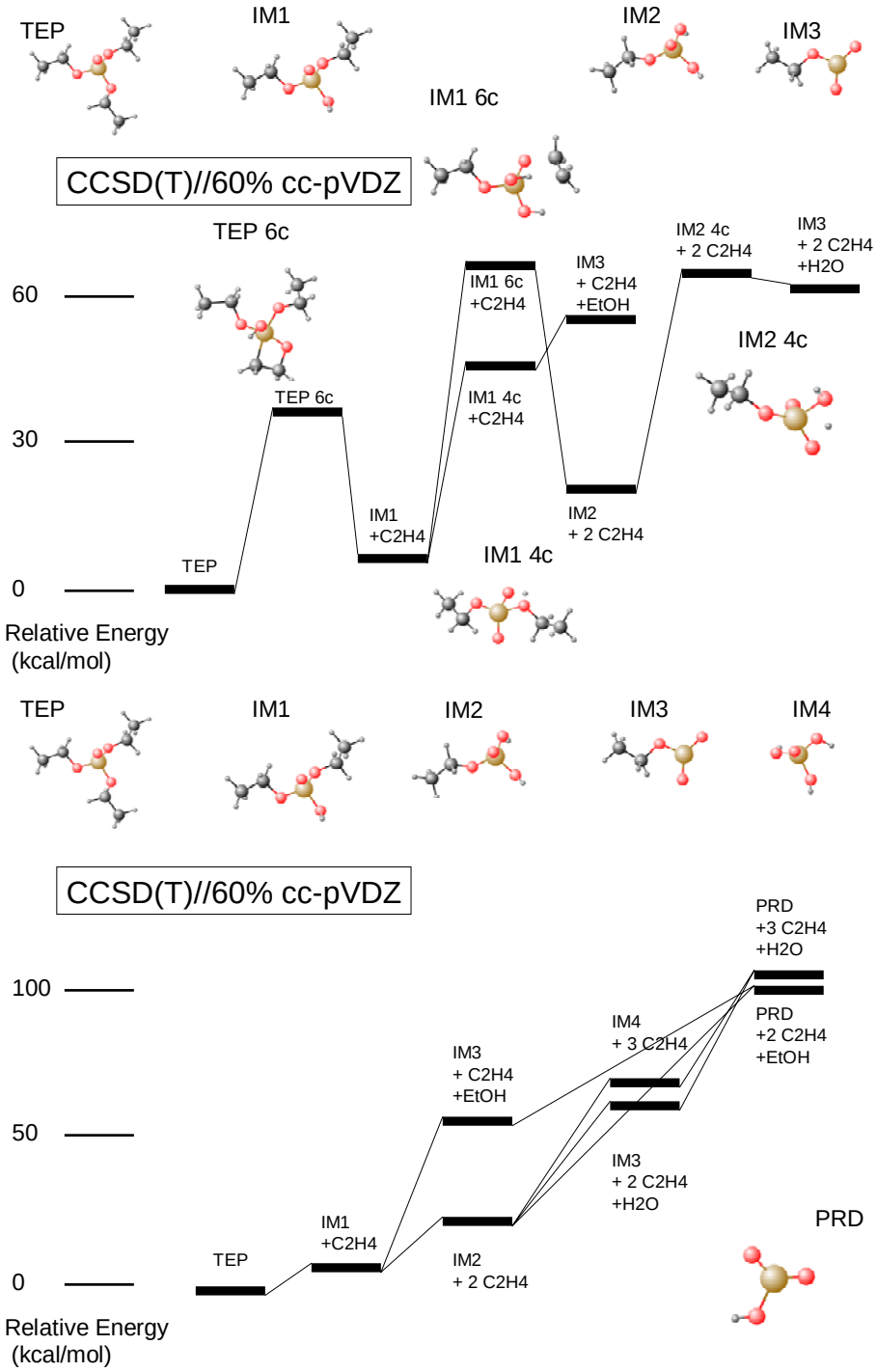
TEP
IM1
IM2
IM3
IM1 6c
CCSD(T)//60% cc-pVDZ
TEP 6c
60
30
0
TEP 6c
IM1 6c
+C2H4
IM3
+ C2H4
+EtOH
IM2 4c
+ 2 C2H4
IM3
+ 2 C2H4
+H2O
IM2 4c
IM1 4c
+C2H4
IM1
+C2H4
IM2
+ 2 C2H4
TEP
IM1 4c
Relative Energy
(kcal/mol)
TEP
IM1
IM2
IM3
IM4
CCSD(T)//60% cc-pVDZ
100
50
0
PRD
+3 C2H4
+H2O
PRD
+2 C2H4
+EtOH
IM4
+ 3 C2H4
IM3
+ C2H4
+EtOH
IM3
+ 2 C2H4
+H2O
IM1
+C2H4
TEP
IM2
+ 2 C2H4
PRD
Relative Energy
(kcal/mol)

Reactant: $P(CH_3)F_2O$ (Difluor)

Energetics: RHF DZP Frozen Core
CCSD: -655.069925 Hartree
CCSD(T): -655.090871 Hartree
ZPE: 30.59 kcal/mol

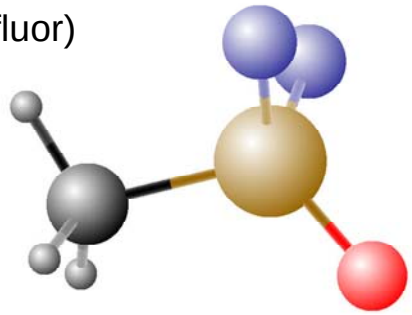

Geometry: RHF CCSD(T) Geom. Opt.
PC Bond (Å): 1.79575
OP Bond (Å): 1.47117
FP Bond (Å): 1.59209
CH Bond (Å): 1.09829
CH' Bond (Å): 1.09792
OPC Angle (Degrees): 119.28267
OPF Angle (Degrees): 115.36170
HCP Angle (Degrees): 109.98315
H'CP Angle (Degrees): 109.06423
FOPC Dihedral (Degrees): +/- 123.09928
HCPO Dihedral (Degrees): 180
H'CPO Dihedral (Degrees): +/- 60
C_s Symmetry

Reaction Thermodynamics

ΔE_{rxn} = 93.85 kcal/mol (CCSD(T))
Endoenergetic

ΔH_{rxn} (0K) = 87.63 kcal/mol (CCSD(T))
Endothermic

Reactant: $P(CH_3)F_2O$ (Difluor)

Energetics: RHF DZP Frozen Core
CCSD: -655.069925 Hartree
CCSD(T): -655.090871 Hartree
ZPE: 30.59 kcal/mol

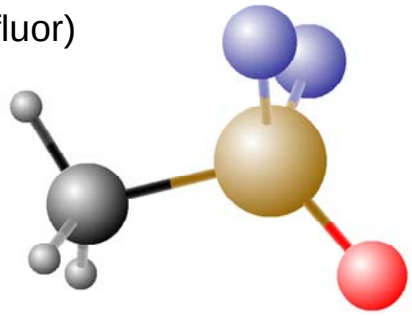

Geometry: RHF CCSD(T) Geom. Opt.
PC Bond (Å): 1.79575
OP Bond (Å): 1.47117
FP Bond (Å): 1.59209
CH Bond (Å): 1.09829
CH' Bond (Å): 1.09792
OPC Angle (Degrees): 119.28267
OPF Angle (Degrees): 115.36170
HCP Angle (Degrees): 109.98315
H'CP Angle (Degrees): 109.06423
FOPC Dihedral (Degrees): +/- 123.09928
HCPO Dihedral (Degrees): 180
H'CPO Dihedral (Degrees): +/- 60
C_s Symmetry

Reaction Thermodynamics

ΔE_{rxn} = 93.85 kcal/mol (CCSD(T))
Endoenergetic

ΔH_{rxn} (0K) = 87.63 kcal/mol (CCSD(T))
Endothermic

DF Vibrations

Symmetry	Frequency (cm^{-1})	Intensity (km/mol)
A"	170.4721	0.0230
A'	265.6011	0.7063
A"	266.4417	0.4517
A'	384.7414	16.3692
A"	388.4039	36.5404
A'	445.9377	102.7625
A'	740.0117	12.0303
A"	844.3198	125.3917
A'	867.6277	170.6884
A'	935.1161	59.0112
A"	953.3815	143.7188
A'	1343.9936	241.8919
A'	1374.6644	88.7446
A'	1466.3581	2.5993
A"	1469.4851	6.7565
A'	3087.2880	0.3102
A'	3195.7313	1.8707
A"	3200.5831	0.8401

Products: CH_3 Doublet Radical

Energetics: RHF DZP Frozen Core
CCSD: -39.719437 Hartree
CCSD(T): -39.722040 Hartree
ZPE: 18.67 kcal/mol

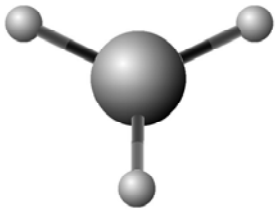

Harmonic Frequencies: CCSD(T)

Symmetry	Frequency (cm^{-1})	Intensity (km/mol)
A1	419.2778	92.4856
A1	1429.9058	2.3868
A1	1429.9058	2.3868
A1	3133.6602	0.0000
A1	3324.0968	11.0383
A1	3324.0968	11.0383

Geometry: RHF CCSD(T) Optimization

CH Bond (Å): 1.08936

D_{3h} Symmetry (C_{2v} Abelian Subgroup)

Products: PF_2O Doublet Radical

Energetics: RHF DZP Frozen Core
CCSD: -615.201307 Hartree
CCSD(T): -615.219262 Hartree
ZPE: 5.70 kcal/mol

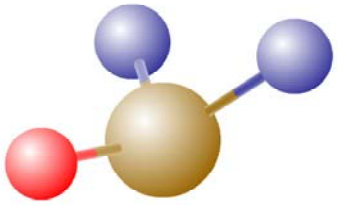

Harmonic Frequencies: CCSD(T)

Symmetry	Frequency (cm^{-1})	Intensity (km/mol)
A''	333.4082	30.3171
A'	345.0059	12.9870
A'	428.9127	68.2681
A'	802.4922	118.8613
A"	849.5265	260.9067
A'	1227.9469	203.8547

Geometry: RHF CCSD(T) Optimization

PO Bond (Å): 1.48748

PF Bond (Å): 1.60053

OPF Angle (Degree): 115.4617

OPFF Dihedral (Angle): -113.5972

C_s Symmetry

The CCSD(T) method, which represents the state-of-the-art for *ab initio* correlated theory that can be applied to molecules of the complexity of TEP, has been augmented by the 60% reduction due to the natural orbital, NO-CCSD(T)

method which has been shown to save ~2^4 in the time for calculations. The optimum way to use this tool is to use a much large basis like cc-pVTZ, and then reduce it by 50%, which will make the calculations take about the same amount of time as the full space CCSD(T) in the cc-pVDZ basis., but as we have shown[94] will retain most of the accuracy of the cc-pVTZ basis., which means the final result will be much better than that for the cc-pVDZ, even though it will take about the same amount of time.

For DF, the direct bond fission requires that we locate the maximum in the have the AG path , which is not fundamentally difficult, but does requires a more complete survey of the PES. This will typically take a few tens of points to provide the information required in RRKM or VTST calculations. These results are shown above.